Uncertainty of Temperature Measurements in Dry Orthogonal Cutting of Titanium Alloys

D. Soler, P. X. Aristimuño, A. Garay, P. J. Arrazola

Manufacturing Department, Faculty of Engineering-Mondragon Unibertsitatea, Mondragon, Spain

Abstract

Infrared radiation thermometer is used to measure the temperature of tool during dry orthogonal cutting of titanium alloys. The accuracy of measured temperature depends on several parameters such as the experimental set-up, physical acquisition data system and physical characteristic of the tool. These parameters are identified, their uncertainty estimated and the way they influence the final temperature discussed.

Keywords: Temperature Measurement, Uncertainty, Infrared, Cutting

1. Introduction

The demand for titanium alloys has increased in recent years [1, 2] because of their outstanding strength-to-weight ratio which makes them very appropriated to be used in aerospace sector. However, titanium alloys are considered as difficult to cut materials for several reasons such as: (i)low conductivity, (ii) High chemical, (iii) low Young Modulus and (iv) workhardening. That is, due to their low thermal conductivity (just 10-20 % of that of steels), only a minor portion of the heat generated during cutting is carried away through by the chips.

Temperatures reached at the tool-chip interface have been recognized as a major factor that influences tool performance [3], because they are a key to understanding the tool wear and final workpiece quality, [4].

Infrared radiation (IR) thermometers [5] have received great attention in recent years as devices for temperature measurement in machining processes,

Email address: dsoler@mondragon.edu (D. Soler)

see for instance [6, 7, 8]. The principal advantages of this technology are that (i) it is non intrusive, and (ii) it allows to determine directly the temperture fields [9]. However, it has some drawbacks such as (i) the difficulty to measure temperature when lubricants are employed, (ii) the equipment cost and (iii) the setting up of the right methodology. In fact, due to the difficulty for measuring temperature with lubricants, dry cutting is the only choice to be considered in nearly all research works.

In general, the temperature of the tool is measured on the side face, and results are reported, in order to visualize how the temperature depends on cutting conditions (feed rate, f, and cutting speed, v_c) and the machined material. Figure 1 shows temperatures reached at the tool rake surface after 5 s of machining time for several titanium alloys,[10, 11, 12], under different cutting conditions: see section 3 for details. It can be observed that the obtained values are between 500 °C and 1200 °C.

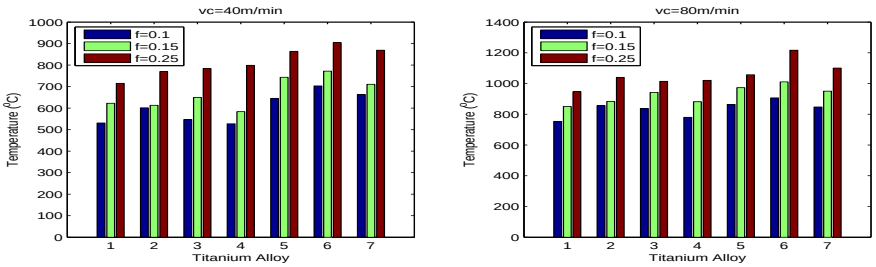

Figure 1: Temperature reached in the tool, during dry orthogonal cutting, for seven different titanium alloys, see section 3 for details. Left plot: v_c = 40 m/min, right plot: v_c = 80 m/min.

When IR technology is used, the measured temperature depends on (i) physical parameters that are difficult to measure, such as the emissivity, and (ii) issues that cannot properly controlled by the operator, like camera calibration. These difficulties lead to a common opinion that temperatures obtained by IR techniques are good enough for comparative analysis but it is not appropriated for reporting quantitative values. When IR technologies are used to report temperature quantitative results of experimental temperature measurements, the uncertainty usually is not provided, [13, 14]. Moreover, when uncertainty is provided, usually the emissivity is identified as the unique uncertainty source, [9, 8], or as the major uncertainty source,[15]. The aim of this paper is to determine the uncertainty of the parameters involved in the whole measuring process that will influence the final measured temperature,

and how these uncertainties influence the final the temperature measurement result.

In order to achieve this objective, the paper is organized as follows: In the next section an introduction of uncertainty theory and some equations that will be used in throughout the paper are presented. In section 3 the experimental set-up is described. In section 4, parameters involved in this experimental set-up are analyzed and their uncertainties are estimated. All results are discussed in section 5 and finally the conclusions are given in section 6.

2. Evaluating Uncertainty

The main objective of this work is to analyze the uncertainty in the measurement of the temperature during dry orthogonal cutting. The standard uncertainty, $u(y)$, of a measurement result, y, is the estimated standard deviation of y. Uncertainty of measurement arises from a number of sources. The evaluation of the combined uncertainty involves first estimating the contribution from each source (the uncertainty budget) and then determining how these will combine to give a combined standard uncertainty. According to [16], uncertainties are grouped into two categories depending on the method used to estimate their numerical values:

- Type A: estimated values are evaluated by statistical methods.
- Type B: estimated values are evaluated by other means.

In this paper evaluated uncertainties are expanded uncertainties with a cover factor of 2,[16]. This means that there is a level of confidence near to 95 % that the true value of measured physical quantity X is in the interval $[x - u(x), x + u(x)]$, where x is the best estimation value of X and $u(x)$ the corresponding uncertainty.

As an example of a Type A evaluation, consider a physical quantity (X) the value of which is estimated from n repeated measurements. The estimated value of X is considered to be the sample mean

$$x = \frac{1}{n} \sum_{k=1}^{n} x_k \tag{1}$$

and the assumed uncertainty $u(x)$ to be associated with x is

$$u(x) = 2u_x = \frac{2s_x}{\sqrt{n}} \tag{2}$$

where s_x is the standard deviation of the experimental sample.

In the case of type B evaluation $u(x) = 2u_x$, where u_x is the standard uncertainty of the measurement [17].

Finally, in many cases, a physical quantity Y is not measured directly but is determined from K other independent physical quantities $X_1, X_2, \ldots X_K$. In that situation, two different cases must be taken into account: when a functional relation is known between Y and $X_1, X_2, \ldots X_K$, and when this relation is unknown. In this work both cases are considered.

In the first case, given $Y = f(X_1, X_2, \ldots, X_K)$, the combined standard uncertainty of the measurement is given by

$$u_c^2(y) = \sum_{j=1}^{K} \left(\frac{\partial f}{\partial x_j} \right)^2 u^2(x_j) \tag{3}$$

where $u(x_j)$ is the standard uncertainty of measured physical quantity X_j estimated by x_j and $\frac{\partial f}{\partial x_j} = \frac{\partial f}{\partial X_j}\Big|_{x_j}$ are the sensitivity coefficients.

In the second case, for the example of a single independent variable X, experimental data pairs (x_i, y_i) are used to fit[1] a non-linear function between them

$$Y = y(a_1, \ldots, a_N, X) \tag{4}$$

where $\{a_j\}$ is a set of N parameters to be determined.

In ordinary measurements the physical quantity X is measured to be x and the function (4) is used to calculate y, the result of the measurement of Y.

Propagation of uncertainty in the case of a non-linear equation in the adjustable parameters is analyzed by Saunders [18]. In the present case the uncertainty of the dependent variable $u(y)$, in the absence of correlations, is given by

$$u^2(y) = \sum_{i=1}^{M} \left(\frac{\partial y}{\partial x_i} \right)^2 u^2(x_i) + \sum_{i=1}^{M} \left(\frac{\partial y}{\partial y_i} \right)^2 u^2(y_i) + \left(\frac{\partial y}{\partial x} \right)^2 u^2(x) \tag{5}$$

[1] In the present paper the unweighted least square method is used to fit the curve.

where $M > N$ is the number of experimental data pairs (x_i, y_i), $u(x_i)$ and $u(y_i)$ are their corresponding standard uncertainties and $u(x)$ the standard uncertainty of experimental data x.

The last term in equation (5) arises when the non-linear equation is used for ordinary measurements, while the first two terms determine the uncertainty of y due to the adjustable parameters, and can be calculated using

$$\frac{\partial y}{\partial x_i} = \sum_{j=1}^{N} [BH^{-1}]_{ij} \frac{\partial y}{\partial a_j} \tag{6}$$

$$\frac{\partial y}{\partial y_i} = \sum_{j=1}^{N} [CH^{-1}]_{ij} \frac{\partial y}{\partial a_j} \tag{7}$$

where $[BH^{-1}]_{ij}$ is the (i,j)th element of the product of two matrices B and H^{-1}, and $[CH^{-1}]_{ij}$ is the (i,j)th element of the product of C and H^{-1}. These matrices are given by

$$B_{ij} = -\left(\frac{\partial y}{\partial x}\frac{\partial y}{\partial a_j}\right)\Bigg|_{x=x_i} + (y_i - y(x))\left.\frac{\partial y}{\partial x \partial a_j}\right|_{x=x_i} \tag{8}$$

$$C_{ij} = \left.\frac{\partial y}{\partial a_j}\right|_{x=x_i} \tag{9}$$

$$H_{kj} = \sum_{i=1}^{M} \left(\frac{\partial y}{\partial a_k}\frac{\partial y}{\partial a_j}\right)\Bigg|_{x=x_i} \tag{10}$$

where $k = 1, \ldots M$.

3. Experimental set-up

In order to be able to compare tool temperatures during dry orthogonal cutting of different titanium alloys, and to reduce the uncertainty sources, some experimental parameters are predetermined:

Sample and cutting conditions:

Samples of different Titanium alloys (see table 1) in the form of cylindrical tube with 48 mm external diameter and 2 mm wall thickness are placed in a Lagun HS 1000 vertical CNC machining center, as is shown on left side of figure 2.

	Material	chemical composition	Heat Treatment
1	Ti64	6 Al 4 V 0.15 Fe 0.18 O	Annealed 705 °C
2	Ti54M	5 Al l0.8 Mo 4 V 0.5 Fe 0.18 O	STA (920 °C (1 h), water quench; 500 °C (4 h))
3	Ti54M	5 Al l0.8 Mo 4 V 0.5 Fe 0.18 O	Annealed 705 °C
4	Ti54M	5 Al l0.8 Mo 4 V 0.5 Fe 0.18 O	β-annealed (990 °C (1 h), water quench; 730 °C, (2 h))
5	Ti 10.2.3	10 V 2 Fe 3 Al 0.13 O	Annelead 760 °C
6	Ti 10.2.3	10 V 2 Fe 3 Al 0.13 O	STA (770 °C (2 h), water quench; 500 °C (8 h); air cool)
7	Ti 10.2.3	10 V 2 Fe 3 Al 0.13 O	STOA (750 °C (2 h), air cool; 565 °C (8 h); air cool)

Table 1: Work piece materials used.

The cutting conditions are controlled by the CNC center. Six different cutting condition are analyzed, corresponding to cutting velocity of 40 m/min and 80 m/min, and feed rate of 0.1, 0.15 and 0.25 mm/rev. Every test is repeated at least three times in order to ensure repeatability, and a new tool is used in every test in order to avoid effects of wear.

Test duration:

At the beginning of a test, the tool is at room temperature. During machining the tool heats up due to work material plastic strain and friction with the tool until it reaches a stationary temperature. This steady state depends on cutting conditions, cut material, and tool geometry.

In previous works [11, 19, 10] it was assumed that the steady state is reached in less than 5 s. For that reason 5 s tests are performed here each experimental condition, analyzing only the lasts 28 ms (100 frames) of cutting.

Tool and Camera:

The tool, a TNMG 160408-23 H13A from Sandvik [2], is prepared to ensure that its radiant surface, $\mathcal{S}$, is perpendicular to the IR camera axis as shown in the right hand part of figure 2.

The camera is a FLIR Titanium 550 M with 320x256 InSb detectors (pixels) and a sensitivity (Noise Equivalent Temperature Difference or NETD) of 20 mK. The camera is equipped with a macroscopic lens giving a spatial resolution of less than 10 μm. A filter allows radiation emitted by $\mathcal{S}$ during the cutting test to be captured in the wavelength range 3.97-4.01 μm.

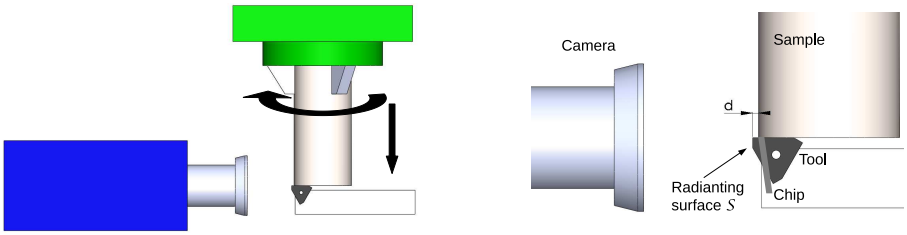

Figure 2: Experimental setup for dry orthogonal cutting. Left:general view; right: the tool radiant surface $\mathcal{S}$ overhanging the chip/tool contact region by a distance d.

The tool surface $\mathcal{S}$ emits infrared radiation that excites the camera's detectors/pixels for some short period of time, integration time (IT). IT must be selected, depending on radiation values, to avoid a non linear detector response. When machining titanium alloys IT is chosen to be 200 μs.

In order to have an as good as possible view of temperature time evolution, it is necessary to have a capture frame rate (fr) as high as possible. In the present case $fr = 3600$ Hz. However, to reach this value of fr the camera resolution must be reduced to 80x64 pixels.

When single value of the temperature is given in section 4, it corresponds, unless otherwise stated, to the average temperature of a slim strip of 300x10μm^2 over the rake face.

The camera position relatively to $\mathcal{S}$, the optical path, is determined by the focal length of the system. However, as can be seen in figure 2, the tool overhangs the chip/tool contact region by a distance d. The value of this distance is approximately $d = 0.3$ mm. However the aggressiveness of some

[2]It is an uncoated carbide tool of K15 type, with rake angle 7 °; cutting edge roundness 34 $\pm$ 2 μ m, and a chip breaker of -15°.

tests can change it. As can be seen in figure 3, the overhang d is measured for every used tool with an optical magnifier.

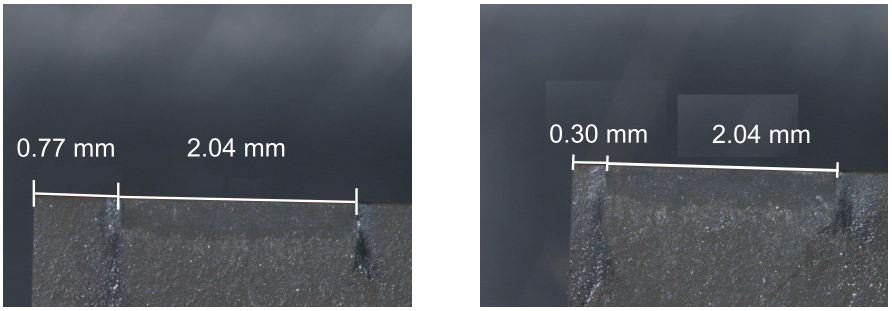

Figure 3: Tool wear is used to measure the distance d. On the left side $d = 0.77$ mm, on the right $d = 0.30$ mm.

It is clear that the heat source is positioned at the contact region between the tool and work-piece. Heat is conducted from there to the surface $\mathcal{S}$ over which the temperature is measured. Therefore the measured temperature is not really the temperature achieved in the cutting zone. While the main objective of these experiments is to measure this temperature, it is not possible to adjust d to zero, because there is a risk of the material not being cut. Moreover, d must be large enough to avoid the chip obstructing the path between $\mathcal{S}$ and the camera.

4. Uncertainty budget

The measurement method, described in section 3, has been kept constant in order to minimize uncertainty sources. In this section an exhaustive analysis of uncertainty sources is given and the corresponding standard uncertainties estimated.

Some uncertainty sources can be identified that are directly related to the experimental set-up used to measure the temperature of the tool in dry orthogonal cutting of titanium alloys some uncertainty sources could be identified: *sample thickness*, *cutting conditions* (f and v_c), *test duration* and *the overhang* d.

The infrared camera does not measure the temperature directly. The IR camera is equipped with a matrix of detectors. Each detector, depending on the amount of photons received, returns an electrical voltage expressed by default in Digital Levels (DLs) depending on a linear transfer function known

as Non Uniform Correction (NUC). The NUC is loaded to the camera before the acquisition process is started. The DL value is not therefore a physically relevant magnitude. A calibration of the camera must be made to relate DLs with real temperatures. To perform a calibration, a blackbody at a known temperature, is placed in front of the camera, allowing the infrared equipment response (DLs) to be related with the blackbody temperature (T_{BB}), commonly called radiance temperature. *The camera calibration* process involves uncertainty sources that must be considered.

To obtain the real temperature (T), it must be taken into account that the tool is not a blackbody. Recall that a blackbody emits more radiation than any other object at the same temperature. The emissivity (ϵ) is the physical parameter that allows T_{BB} to relate to T. When Wien approximation is valid, the following relationship can be written between T and T_{BB} [20]

$$\frac{1}{T} = \frac{1}{T_{BB}} + \frac{\lambda}{C_\omega} \ln(\epsilon) \tag{11}$$

where $C_\omega = 14389$ Kμm and ϵ is the emissivity of a surface at the λ wavelength. Therefore, the uncertainty of th *emissivity* must be estimated.

Finally, when the measurement is been made, assuming the tool is an opaque object, the radiation detected by the camera can have different origins: the radiation emitted by the tool, that is related to the tool temperature; the radiation reflected by the tool (*ambient temperature* uncertainty source); and the radiation coming out of the tool (*size-of-source effect*). These uncertainty sources will be analyzed in subsection 4.4, under the title of environmental uncertainties.

4.1. Uncertainty sources related to the experimental set-up

Workpiece thickness:

As can be seen in figure 4, sample thickness affects the measured temperature. However, as previously commented in section 3, all the samples have the same thickness in these tests, it is measured with a Type B uncertainty of 0.005 mm. The authors therefore consider no relevant uncertainty comes from this parameter in the final temperature estimate.

Cutting conditions:

As with workpiece thickness, tool temperature is strongly dependent on cutting conditions, see figure 1. However, the CNC machining center has a good control of f and v_c and the uncertainty of these parameters will not be relevant to the final temperature.

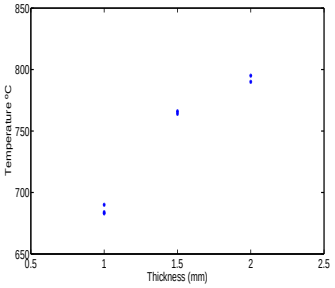

Figure 4: Maximum temperature on the rake face as a function of sample thickness when machining a titanium alloy (cutting speed 80 m/min, feed 0.1 mm/rev).

Test duration:

Figure 5 shows DL values for one pixel on the rake face during the whole test and over the last 300 frames. Although the steady state was not reached in this experiment, the experimental procedure of constant test duration justifies the comparison between different tests. Experiment duration could introduce an uncertainty component into the final temperature estimate but will not be considered.

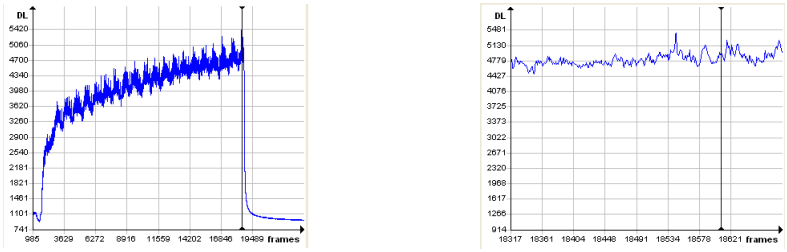

Figure 5: Digital Level vs. frame number for a titanium alloy: left: whole test (left); right: the last frames.

The overhang (d):

In order to quantify the influence of d on final temperature, some experimental tests have been carried out machining a titanium alloy (Ti54M, [11]). The the obtained dependence is shown in figure 6.

Experimental data can be fitted using the three parameter non-linear function

$$T(d) = a_1 e^{a_2 d} + a_3 d. \tag{12}$$

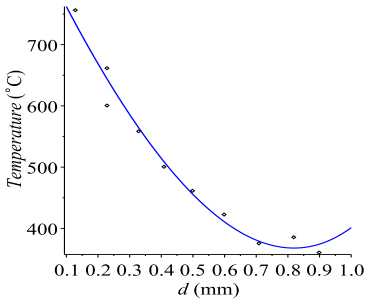

Figure 6: Temperature vs. d when machining a titanium alloy: Experimental data and fitting function (12).

The least-square fitting is used, and obtained parameters are: $a_1 = 865$, $a_2 = 0.990$ and $a_3 = -1.93 \cdot 10^3$.

By means of equations (6) to (10) it is possible to calculate the uncertainty due to this relationship. It is necessary to estimate the uncertainty in d and in the temperature. Figure 7 shows the estimated relative combined standard uncertainty in temperature, $u_r(T)$, assuming a type B standard uncertainty $u(d) = 0.015$ mm and $\frac{u(T)}{T} = 10\%$. The estimated uncertainty is about 4.6 % when d is 0.3 mm.

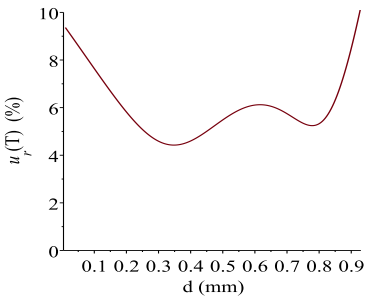

Figure 7: Uncertainty in the temperature due to the 3-parameter adjustment given by equation (12) for the experimental data plotted in figure 6.

This uncertainty implies that an uncertainty of 5% in d leads to an uncertainty of 4.6 % in temperature at $\mathcal{S}$. In ref. [21] it is analyzed the effect of d when temperature in chip/tool contact area is estimated, being the divergence between two temperature of 30 % or more.

4.2. Uncertainty sources related to the camera calibration process

The camera position relative to the emitting surface, the capture frame rate, the integration time and the number of pixels, are parameters that affect the camera DL response, because of previously the loaded NUC. Figure 8 there is a clearly shows a dependence between camera response and the uploaded NUC. Even when the only difference between two pictures is the window's size, the central response differs $\sim$ 1000 DLs.

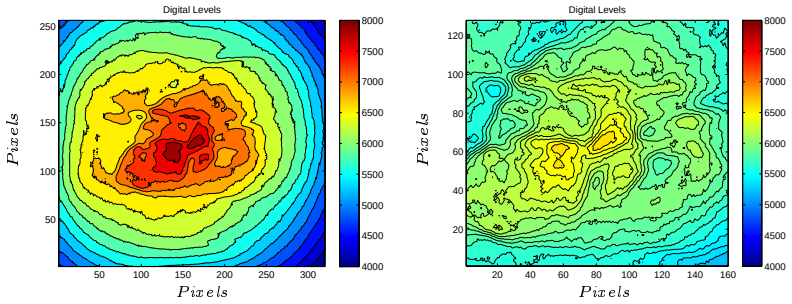

(a) (b)

Figure 8: Camera response when placed in front a black body at 600 °C with an integration time of 200 μs. (a) performed using the NUC corresponding to big window size, and (b) to medium size. DLs by up to 1000 units.

For this reason, camera calibration must be carried out in the same conditions as the experiments. The present calibration has been performed in a pixel by pixel process, following the procedure:

- Define a set of temperatures at regular intervals over the dynamic range, in this case[3] from 300 to 750 °C, at intervals of 50 °C.
- Place a black body source (an Isotech Pegasus 'R') in front of the camera and make a film at each temperature lasting for 100 frames.
- At each temperature (T_{BB}), compute the average signal (S) and the corresponding standard deviation for every pixel and the corresponding in order to estimate $u(S)$ using equation (2).

[3]It might seem these values are out of range (see figure 1), but taking into account that real temperature must be calculated with the equation (11) and the typical value of $\epsilon \approx 0.37$ they are not.

- Use pairs (S, T_{BB}) of every pixel to fit an interpolating function, the calibration curve.

In the literature [7, 22, 18], there are several types of non linear functions with three fitting parameters that relate S and T_{BB}. In this work, the transfer function used is [23]:

$$T_{BB} = \alpha_1 \ln(S + \alpha_2) + \alpha_3 \tag{13}$$

Figure 9(b) shows a typical image of the surface $\mathcal{S}$. A single pixel is highlighted (the black square). Figure 9(a) shows, for that pixel, the obtained relationship between S and T_{BB}, as well as the fitted curve using function (13), and the fitted curve using the Plank version of Sakuma-Hattori equation [24].

$$S - H: \quad S = a_1/(e^{c_2/(a_2 T + a_3)} - 1) \tag{14}$$

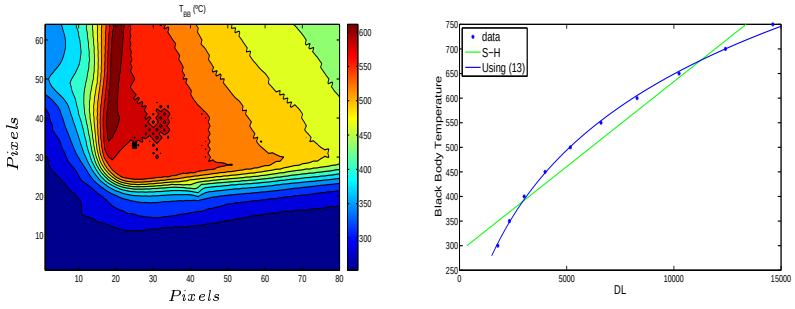

(a) (b)

Figure 9: (a) Typical picture of the tool side face during orthogonal cutting of titanium alloy. (b) Transfer functions fitted to relate camera response in DLs to black body temperature (T_{BB}), corresponding to the pixel highlighted in the picture (a).

The standard uncertainty in T_{BB} due to uncertainty in the calibration data can be estimated for each pixel using equations (5) to (10).

Figure 10 shows the relative standard uncertainty for the pixel in figure 9. To obtain this curve, the type B standard uncertainty in calibration temperature measurement is estimated to be 5 °C. the type A uncertainty in DLs is taken to be 0.05%. This is the maximum statistical uncertainty, based on equation (2), in the pixel signal from calibration films.

In figure 10, the relative standard uncertainty in T_{BB} due to the calibration fitting is less than 0.6% for T_{BB} between 400 and 750 °C. The calibration

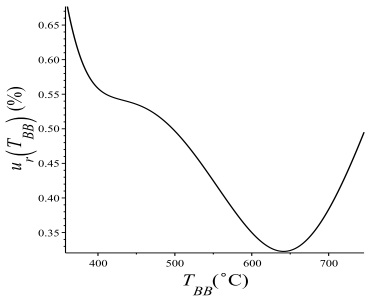

Figure 10: Estimated relative uncertainty in T_{BB} due to the accuracy of the calibration fitting showed in figure 9.

curves are used for each pixel and frame to compute T_{BB} in all tests. However in an ordinary test the uncertainty in the DL signal is greater than 0.05%. Moreover, the uncertainty in DLs can rise to 2% for the pixels located in the rake face. In that case the most relevant factor in equation (5) is the last one, not included in figure 10. When a relative standard uncertainty in DLs of 2% is assumed, the total uncertainty due to the calibration is shown in figure 11. It is smaller than 1.1%. The decreasing trend of the % uncertainty with the temperature is because the mentioned last term of equation (5) leads to an almost constant uncertainty of about 4.5 °C for the corresponding range of DLs.

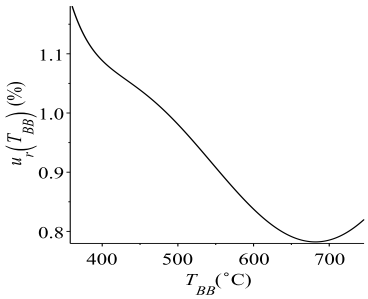

Figure 11: Estimated total relative standard uncertainty in T_{BB} due to the accuracy of the calibration fitting and the uncertainty in DL measurements in an ordinary test.

4.3. Uncertainty sources related with emissivity

The true temperature T, can be estimated from T_{BB} through the equation (11). Emissivity, ϵ, of the tool is measured in vacuum using a FTIR [25].

Figure 12 shows the mean values of ϵ of the SANDVIK TNMG 160408-23 H13A tool, obtained at different wavelengths between 3.97 and 4.01 μm at the corresponding radiance temperature. The curve is the fitting of a 3rd degree polynomial in order to obtain the emissivity dependence on T_{BB}.

$$\epsilon = -2.17 \cdot 10^{-9} T_{BB}^3 + 3.02 \cdot 10^{-6} T_{BB}^2 - 1.34 \cdot 10^{-3} T_{BB} + 0.563 \qquad (15)$$

This polynomial is used to compute the emissivity of every pixel of each frame at a given T_{BB}.

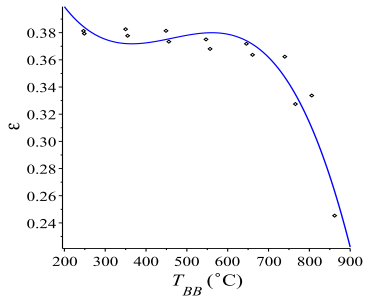

Figure 12: Experimental points obtained by FTIR, and a 3rd degree fitted polynomial.

In the same way as with the calibration curve, the uncertainty of the emissivity caused by the uncertainty of the experimental points appearing in figure 12 can be computed. The corresponding uncertainty curve is shown in figure 13(a). This curve has been obtained taking into account that FTIR measurement has type B uncertainties of $u_r(\epsilon) = 0.5\%$ and $u(T_{BB}) = 5$ °C.

However, in an ordinary experiment, the uncertainty in T_{BB} must be calculated from $u(DL)$ given by the camera when using the corresponding calibration. In section 4.2 it is shown that a value of 1.1% could be taken for this uncertainty.

Figure 13(b) shows total relative standard uncertainty of the emissivity versus T_{BB}. If $T_{BB} < 650$ °C, this uncertainty is lower than 0.5 %.

In order to apply the correct emissivity to pixel T_{BB} reading, it has to be determined, in the IR picture, whether the pixel is part of the tool, the chip, the work, or the background image. During the cutting process, the tool is at higher temperature than the work and the background and the radiation variation is smaller in the tool than in the chip. By considering the temperature and the standard deviation of DLs signal, it is possible to identify the surface of the tool in an IR picture.

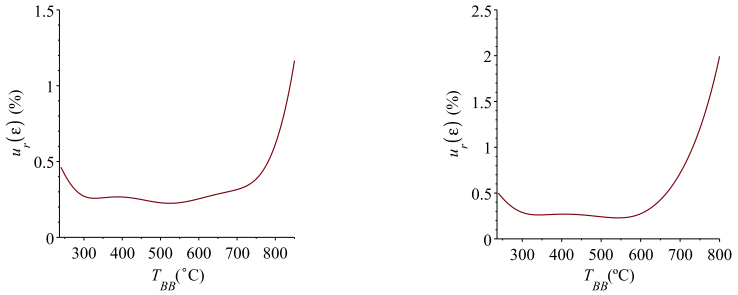

(a) (b)

Figure 13: (a) Relative error of emissivity vs T_{BB} due to the uncertainty of experimental data of figure 12. (b) Total relative error of emissivity vs. T_{BB}.

However, it is difficult to determine exactly the position of the rake face, i.e., where is the boundary of he tool. This is important because the rake face contains most interesting points. When in section 4.2 an uncertainty of 2% in DL reading is assumed, it corresponds to the mean of maximum values obtained for the $u(DL)$ of the rake face pixels.

For each pixel, the polynomial presented in equation (15) is used to calculate the emissivity corresponding to the measured radiance temperature. Then equation (11) is used to estimate T. The equation (3) must be used to compute uncertainty of T. This leads to

$$\frac{u(T)}{T} = T\left(\frac{1}{T_{BB}}\frac{u(T_{BB})}{T_{BB}} + \frac{\lambda}{C_\omega}\frac{u(\epsilon)}{\epsilon}\right) \tag{16}$$

As mentioned before, $\frac{u(T_{BB})}{T_{BB}}$ is estimated in section 4.2 to be about 1.1%. As it can be seen in figure 12 when T_{BB} is in the range 220 to 750 °C then ϵ is in the range [0.35,0.39]. From equation (11) these values leads to T being in the range of temperatures reached in the experiments (figure 1). Therefore it is justified, see for instance figure 13(b), to limit $\frac{\Delta\epsilon}{\epsilon}$ to about 1 %.

Figure 14 shows the relative standard uncertainty, from equation (16), of the temperature of the tool as a function of T.

4.4. Environmental uncertainties

As commented on section 3, in order to be able to measure the time evolution of the temperature, camera field of view is reduced from 360x256 to 80x64 pixels. The pixels used are those in the central region of field of

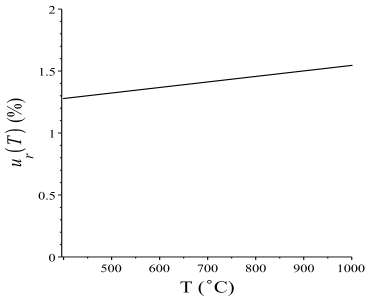

Figure 14: Relative standard uncertainty of final temperature vs. final temperature calculated by propagating emissivity and T_{BB} uncertainties from (16).

view. Only a small part of the target (tool surface $\mathcal{S}$) is imaged. Moreover, this part is at highest temperature, for this reason the *size-of-source effect* is dismissed in this case. The radiation detected by the camera is supposed to have two origins: the radiation emitted by the tool and the radiation reflected by the tool.

$$S(T_m) = \epsilon S(T_t) + (1 - \epsilon) S(T_{amb}) \tag{17}$$

Equation (17) states that the detected signal ($S(T_m)$), used to estimate the temperature of the tool during the cutting process, is the addition of ($S(T_t)$), the radiation emitted by the tool, and $S(T_{amb})$ the radiation reflected by the tool.

If the emissivity (ϵ) is large enough, near to 1, and when the surrounding temperature (about 20 °C), is much smaller than the target temperature, the second term of equation (17) is negligible in comparison with the first. However, tools used to machine titanium alloys have quite small emissivity, close to 0.37, and the ambient temperature effect must be taken into account. In this situation, the second term in equation (17) can be used to estimate the uncertainty in $S(T_m)$ from neglecting the reflected radiation.

$$u(S) = (1 - \epsilon) S(T_{amb}) \tag{18}$$

Equation (13) relates radiation signal to radiance temperature (T_{BB}). A straight forward calculation, using equation (3), allows the relative uncertainty in the assumed T_{BB} of the tool to be computed. Figure 15(a) shows this uncertainty.

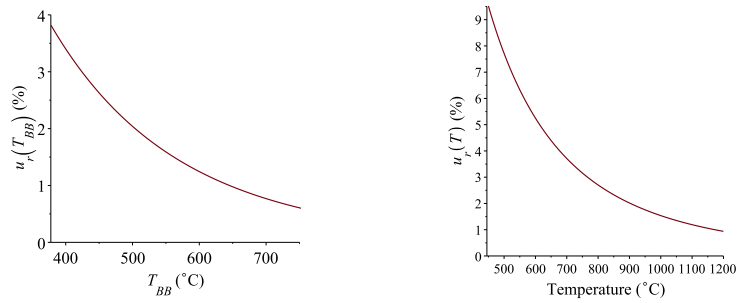

(a) (b)

Figure 15: Relative uncertainty due to not considering reflected radioation of (a) the radiance temperature T_{BB}, and (b) the tool temperature T.

Equation (11) relates T_{BB} to the real temperature of the tool (T), therefore, again using (3), it is possible to propagate the uncertainty in T_{BB} into T. This leads to relative uncertainty plotted in figure 15(b).

5. Discussion

In previous sections the sources of uncertainty in tool temperature during dry orthogonal cutting of titanium alloys are analyzed. Table 2 summarizes the considered uncertainty sources and propagated effects.

Figure 6 shows that small variations in the value of d lead to a large variation in the temperature. Therefore, in spite of good accuracy in d measurement, the uncertainty of T due to this parameter is not negligible. The value of $u(d) = 4.6\%$ in table 2 corresponds to $d = 0.3$ mm in figure 7. However, it must be taken as an approximate value because the curve of figure 12 is specific to machining Ti54M. For more accurate uncertainty estimation, curves should be obtained for different material, with more experimental values close to $d = 0.3$ mm.

As discussed in section 4.3, the uncertainty in the camera in DLs readings is estimated to be approximately of 2%. This uncertainty is used in sections 4.2 and 4.3 to compute the last term of equation (5), to estimate the uncertainties $u(T_{BB})$ and $u(\epsilon)$ (figures 11 and 13(a) respectively). Equation (16) propagates these uncertainties to the uncertainty shown in figure 14. $u(T_{BB})$ contributes about of 1.2% when $T = 500$ °C and about 1.4% when $T = 1000$ °C; $u(\epsilon)$ contributes about 0.1% for $T = 500$ °C and 0.25% when $T = 1000$ °C.

Uncertainty source	$\frac{\Delta T}{T}$ (%)
Sample Thickness	negligible
Cutting conditions	negligible
Test Duration	negligible
d parameter: $u(d)$	4.6
Radiance temperature: $u(T_{BB})$	1.2 - 1.4
Emissivity: $u(\epsilon)$	0.1 - 0.25
Size-of-source effect	negligible
Ambient Temperature: $u(S)$	1.5 - 9

Table 2: Summary of considered uncertainty sources.

The small value of the emissivity of the tool implies a relative uncertainty in temperature due to not considering reflected radiation. Figure 15(b) shows this uncertainty. It decreases rapidly as temperature grows. It is possible to include measurements in the experimental set-up to estimate the radiation reflected by the tool. In that case, the signal S could be corrected and the uncertainty from this reason could be strongly reduced. Another possibility is to paint the tool in order to increase its emissivity.

6. Conclusions

An experimental set-up to measure the tool temperature during dry orthogonal cutting using infrared techniques is described. The present work analyzes the case when machined the material is a titanium alloy. However, the same procedure can be followed for other materials. The uncertainty in the temperature measured by this method is analyzed and discussed. The most relevant results are:

- The estimated uncertainty of the Digital Levels is about 2% in all the examples analyzed, and the highest uncertainty occurs with the pixels placed positioned at the rake face.
- This uncertainty leads to an almost constant uncertainty in the final temperature of approximately 1.6%.
- Due to the small value of the tool emissivity, the ambient temperature is a relevant factor for low temperatures (near 500 °C), rising to 9 %, but

this factor falls to 1.5% for hard cutting conditions when temperature grows up to 1000 °C.

- The distance d between the external diameter of the work and the surface where the temperature is measured strongly influences the precision of the measured temperature. For this reason, an extra uncertainty of 4.6% has to be added to the global uncertainty of the temperature.

- Therefore, the uncertainty in temperature measurements is about 15 % for temperatures near to 500°C and about 8% for temperatures near to 1000°C.

Acknowledgements

The authors thank the Basque government for the financial support given to the projects PROFUTURE I (code IE10-271) and PROFUTURE II (code IE11-308))and the Spanish government for support to the projects INPRORET (IE12-342) and METINCOX (DPI2009-14286-C02-0 and PI-2010-11).

The authors would also like to thank Dr. T. Childs of School of Mechanical Engineering, University of Leeds, for his allays interesting comments.

References

[1] ResearchInChina. Global and china titanium industry report, 2009-2010. http://www.researchinchina.com/Htmls/Report/2010/5941.html, 2010.

[2] U.S. Geological Survey. Mineral commodity summaries 2013, 2013.

[3] G. Sutter, L. Faure, A. Molinari, N. Ranc, and V. Pina. An experimental technique for the measurement of temperature fields for the orthogonal cutting in high speed machining. *International Journal of Machine Tools and Manufacture*, 43(7):671 – 678, 2003.

[4] MA Davies, T. Ueda, R. M'saoubi, B. Mullany, and AL Cooke. On the measurement of temperature in material removal processes. *CIRP Annals-Manufacturing Technology*, 56(2):581–604, 2007.

[5] A. Rogalski. Infrared detectors: an overview. *Infrared Physics & Technology*, 43(3-5):187–210, 2002.

[6] J. Pujana, L. Del Campo, RB Perez-Saez, MJ Tello, I. Gallego, and PJ Arrazola. Radiation thermometry applied to temperature measurement in the cutting process. *Measurement Science and Technology*, 18:3409, 2007.

[7] R. M'Saoubi and H. Chandrasekaran. Investigation of the effects of tool micro-geometry and coating on tool temperature during orthogonal turning of quenched and tempered steel. *International Journal of Machine Tools and Manufacture*, 44:213 – 224, 2004.

[8] R.C Dewes, E Ng, K.S Chua, P.G Newton, and D.K Aspinwall. Temperature measurement when high speed machining hardened mould/die steel. *Journal of Materials Processing Technology*, 92-93(0):293 – 301, 1999.

[9] R M'Saoubi, C Le Calvez, B Changeux, and J L Lebrun. Thermal and microstructural analysis of orthogonal cutting of a low alloyed carbon steel using an infraredŮcharge-coupled device camera technique. *Proceedings of the Institution of Mechanical Engineers, Part B: Journal of Engineering Manufacture*, 216(2):153–165, 2002.

[10] M. Armendia, A. Garay, L.M. Iriarte, and P.J. Arrazola. Comparison of the machinabilities of ti6al4v and timetal 54m using uncoated wc-co tools. *Journal of Materials Processing Technology*, 210(2):197 – 203, 2010.

[11] Navneet Khanna, Ainhara Garay, Luis M. Iriarte, Daniel Soler, Kuldip S. Sangwan, and Pedro J. Arrazola. Effect of heat treatment conditions on the machinability of ti64 and ti54m alloys. *Procedia CIRP*, 1(0):477 – 482, 2012.

[12] Navneet Khanna and Kuldip S Sangwan. Machinability study of α/β and β titanium alloys in different heat treatment conditions. *Proceedings of the Institution of Mechanical Engineers, Part B: Journal of Engineering Manufacture*, 227(3):357–361, 2013.

[13] W Grzesik, P Kiszka, D Kowalczyk, J Rech, and Ch Claudin. Machining of nodular cast iron (pf-nci) using cbn tools. *Procedia CIRP*, 1:483–487, 2012.

[14] R M'saoubi, JL Lebrun, and B Changeux. A new method for cutting tool temperature measurement using ccd infrared technique: influence of tool and coating. *Machining Science and Technology*, 2(2):369–382, 1998.

[15] MA Davies, H. Yoon, TL Schmitz, TJ Burns, and MD Kennedy. Calibrated thermal microscopy of the tool–chip interface in machining. *Machining science and technology*, 7(2):167–190, 2003.

[16] IEC Bipm, ISO IFCC, OIML IUPAC, and ISO OIML. Guide to the expression of uncertainty in measurement. *ISO, Geneva*, 1993.

[17] Barry N. Taylor. *Guidelines for Evaluating and Expressing the Uncertainty of NIST Measurement Results (rev. Ed.)*. DIANE Publishing, November 2009.

[18] P. Saunders. Propagation of uncertainty for non-linear calibration equations with an application in radiation thermometry. *Metrologia*, 40:93–101, 2003.

[19] M. Armendia, A. Garay, A. Villar, MA Davies, and PJ Arrazola. High bandwidth temperature measurement in interrupted cutting of difficult to machine materials. *CIRP Annals-Manufacturing Technology*, 59(1):97 – 100, 2010.

[20] Peter Saunders. *Radiation Thermometry: Fundamentals and Applications in the Petrochemical Industry*, volume TT78. SPIE Press, 2007.

[21] D. Soler, T. H. C. Childs, and P. J. Arrazola. A note on interpreting tool temperature measurements from thermography. *Machining Science and Technology*, 2013.

[22] F. Sakuma and S. Hattori. Establishing a practical temperature standard by using a narrow-band radiation thermometer with a silicon detector. *Temperature: Its Measurement and Control in Science and Industry*, 5:421–427, 1982. ID: 22259.

[23] PJ Arrazola, I. Arriola, MA Davies, AL Cooke, and BS Dutterer. The effect of machinability on thermal fields in orthogonal cutting of AISI 4140 steel. *CIRP Annals-Manufacturing Technology*, 57(1):65–68, 2008.

[24] P. Saunders, J. Fischer, M. Sadli, M. Battuello, CW Park, Z. Yuan, H. Yoon, W. Li, E. Van Der Ham, F. Sakuma, et al. Uncertainty budgets for calibration of radiation thermometers below the silver point. *International Journal of Thermophysics*, 29(3):1066–1083, 2008.

[25] L. del Campo, R.B. Pérez-Sáez, X. Esquisabel, I. Fernández, and M.J. Tello. New experimental device for infrared spectral directional emissivity measurements in a controlled environment. *Review of Scientific Instruments*, 77:113111, 2006.